Separation and Purification Technology 349 (2024) 127584

Contents lists available at ScienceDirect

Separation and Purification Technology

journal homepage: www.elsevier.com/locate/seppur

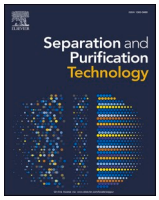

Comparison of the effect of topology type and linker composition of zeolitic imidazolate framework fillers on the performance of mixed matrix membranes in CO_2/N_2 separation

Qian Jia [a,1], Elsa Lasseuguette [b,1], Maria-Chiara Ferrari [b,*], Paul A. Wright [a,*]

[a] EaStCHEM School of Chemistry, University of St Andrews, Purdie Building, North Haugh, St Andrews KY16 9ST, United Kingdom
[b] School of Engineering, University of Edinburgh, Robert Stevenson Road, Edinburgh EH9 3FB, United Kingdom

ARTICLE INFO

Keywords:
Mixed matrix membranes
Zeolitic imidazolate frameworks
ZIFs
CO_2 separation

ABSTRACT

Mixed matrix membranes (MMMs) combine the high separation performance of porous materials with the processibility of polymers and so possess potential for carbon capture from CO_2-containing gas streams. Zeolitic imidazolate frameworks (ZIFs) are promising candidates as molecular-sieve fillers in MMMs due to their tunability and ease of synthesis. We have compared four ZIFs, all as nanoparticles of similar sizes (*ca.* 400 nm), as MMM fillers, to investigate the effects of ZIF structure and chemistry on MMM performance of pure gas (CO_2, N_2) permeation under the same conditions. The chosen ZIFs include two that exhibit strong CO_2 adsorption (hybrid ZIF-7/COK-17 and ZIF-94) and two that have higher pore volumes but weaker CO_2 interactions (ZIF-8 and a hybrid ZIF-11/ZIF-71). The hybrid ZIF-7/COK-17 and ZIF-94 are structurally related to ZIF-7 (rhombohedral **sod** topology) and ZIF-8 (cubic **sod**), respectively, via partial or complete substitution of benzimidazole or 2-methylimidazole by 4,5-dichloroimidazole or 4-methyl-5-imidazolecarboxaldehyde, while the hybrid ZIF-11/ZIF-71 has the **rho** topology but the same composition as the ZIF-7/COK-17 hybrid. In the first part of the comparative study, MMMs based on two types of commercial polymers, Matrimid®5218 and PEBAX-MH1657, were prepared containing the ZIF-7/COK-17 hybrid and also with ZIF-94. ZIF-94 shows much better compatibility with the polymers, forming homogeneous dispersions at all loadings attempted ($\leq$35 % wt%) whereas the hybrid shows inhomogeneity above 12 wt% in each case. At 12 wt% loading, both fillers show an increase in CO_2 permeability at 1.2 bar and 293 K compared to the pure membrane (in PEBAX, this increases from 49.5 to 60 and 68 Barrer) which is the result of increased solubility compensating for decreased diffusivity, and this improvement in permeability continues to increase at the higher levels of loading possible with ZIF-94. ZIF-7/COK-17 in PEBAX show higher selectivity, achieving a calculated CO_2/N_2 selectivity up to 70. Further investigation of CO_2 and N_2 permeation on MMMs with the four ZIFs at 12 wt% in PEBAX-MH1657 showed a clear distinction between the ZIF-94 and ZIF-7/COK-17 MMMs (which show higher membrane solubilities but lower diffusivities) compared to ZIF-8 and ZIF-11/ZIF-71 MMMs. At the loading chosen, the CO_2 permeability increase achieved by the four ZIFs over PEBAX-MH1657 increases in the order ZIF-11/-71, ZIF-7-COK-17 (ca. 60 Barrer) < ZIF-94 (68) < ZIF-8 (81), reflecting the complex interplay between CO_2 solubility (increasing with interaction strength) and diffusivity (increasing with available cage and window size). The calculated CO_2/N_2 selectivity is highest for the hybrid ZIF-7/COK-17 membrane (70), which is attributed to molecular sieving effects in the rhombohedral **sod** structure.

1. Introduction

The use of polymeric membranes for gas separation has seen significant growth in industrial sectors since the 1980s due to their small footprint and low-energy consumption [1]. However, these membranes generally suffer from ageing issues and the Robeson upper limit, where improvements in selectivity come at the expense of gas permeability, and vice versa [2,3]. Moreover, gas molecules such as CO_2 can induce

* Corresponding authors.
E-mail addresses: m.ferrari@ed.ac.uk (M.-C. Ferrari), paw2@st-andrews.ac.uk (P.A. Wright).
[1] These authors contributed equally to this work.

https://doi.org/10.1016/j.seppur.2024.127584
Received 19 September 2023; Received in revised form 2 April 2024; Accepted 18 April 2024
Available online 19 April 2024

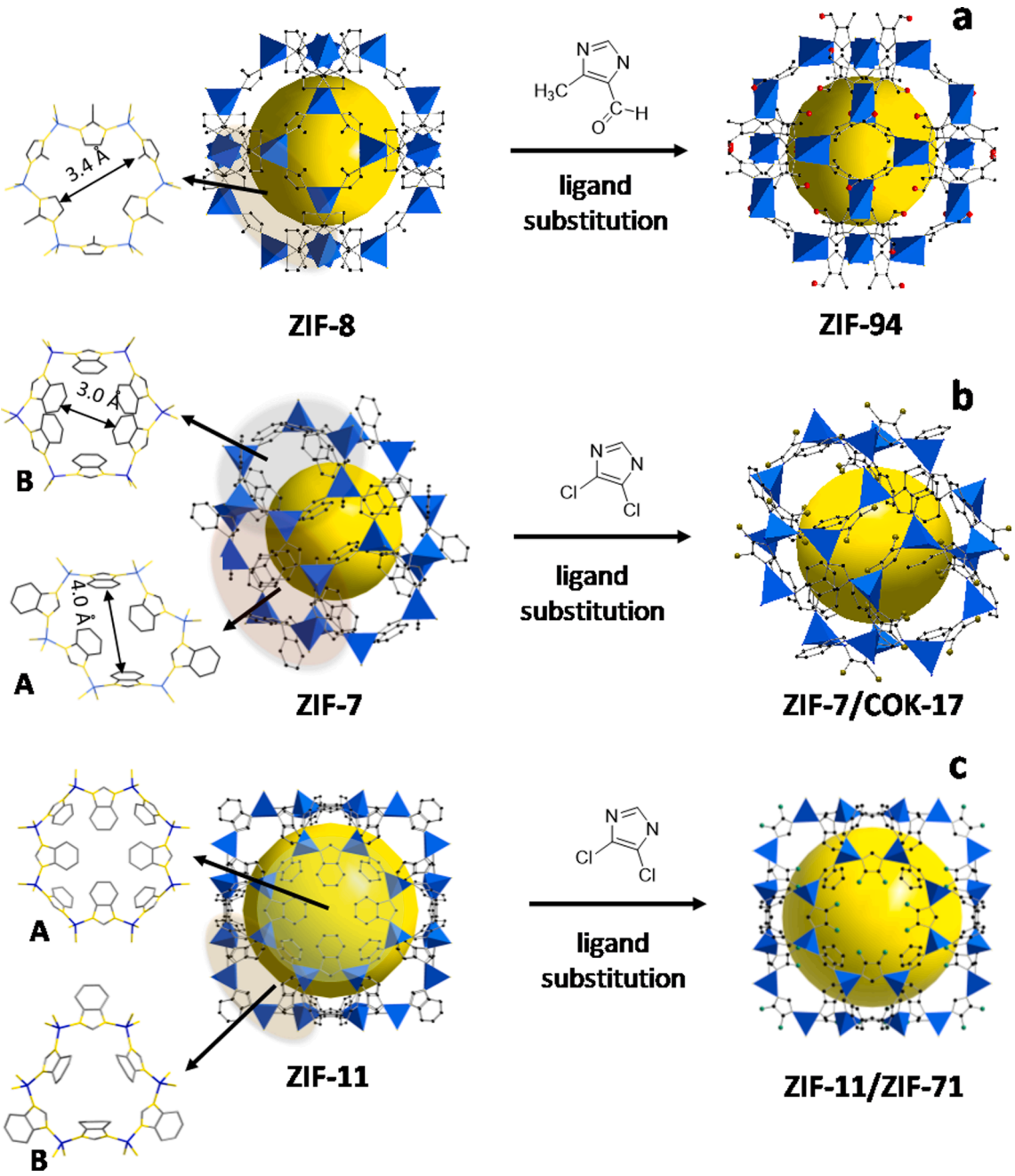

Fig. 1. Schematic formation of (a) ZIF-94 by replacing methylimidazole in ZIF-8 with 4-methyl-5-imidazolecarboxaldehyde; (b) ZIF-7/COK-17 by partially substituting benzimidazole (BzIm) in ZIF-7 with 4,5-dichloroimidazole (dcIm); (c) hybrid ZIF-11/ZIF-71 by partially substituting BzIm in ZIF-11 with dcIm. Possible adsorption sites in ZIF-7, ZIF-8 and ZIF-11 are grey-shaded and shown alongside the cage: ZIF-7 and ZIF-11 have two types of sites (A and B), and ZIF-8 only one.

polymer swelling and plasticisation, negatively impacting membrane performance [4,5]. To overcome these challenges, a mixed matrix approach incorporating porous fillers, such as zeolites, activated carbon, and metal organic frameworks (MOFs), has emerged as a promising solution [6].

MOFs excel as fillers in membranes because they can have a pore size that can introduce selectivity as molecular sieves and they exhibit great structural and chemical tunability that can give a wide range of selective adsorption sites [7]. Additionally, the chemical compatibility between the organic linkers at the surfaces of MOF filler particles is greater than that of purely inorganic filler particles, leading to improved particle dispersion and interfacial contact [8–11].

Zeolitic imidazolate frameworks (ZIFs) are one family of MOFs that has found extensive application in mixed matrix membranes (MMMs), particularly considering CO_2 separation from N_2 in flue gases [12–16]. These have a zeolite-like topology constructed from metal nodes (Zn^{2+} and Co^{2+}) which are connected tetrahedrally via imidazolate linkers [17,18]. For example, ZIF-7 and ZIF-8, in which Zn^{2+} cations are linked by benzimidazole (BzIm) and 2-methylimidazole (MeIm), respectively, display the **sod** (sodalite) topology and have been widely employed in membranes for gas separations [15,19,20]. ZIF-8 possesses cubic symmetry and ZIF-7 rhombohedral symmetry, distorted away from cubic due to steric interactions of the BzIm linker (Fig. 1).

ZIFs demonstrate good stability in membranes, considerable chemical and structural tunability deriving from the use of different imidazolate linkers and importantly can be prepared as nanocrystals that are readily dispersed in polymer matrices [21–24]. Most studies of ZIFs within MMMs have centred on ZIF-8 and ZIF-7 and their functionalised

variants, [19,25–27] although there are some reports on ZIFs with the **rho** or **cha** topology types, where the three dimensional pore connectivity is via 8-membered, rather than 6-membered rings [28–31].

Some previous work has compared a wide range of MOF MMMs and analysed the impact of many different variables via data mining and a resultant mathematical model [32]. This indicated the contribution of MOF fillers to membrane performance depends strongly on polymer properties, as well as MOF properties such as pore size, BET surface areas, particle size and functionality. However, due to a very disparate set of MOF chemistries (ZIF-8, UiO-66, MOF-5 and MIL-53-based MMMs (648 sets)), the specific effects of structural features of similar MOF fillers are obscured in this work. By contrast, a recent paper on the use of MOF-808 in MMMs with Matrimid has used the same parent MOF crystals and functionalised them with different ligands, changing pore volume and functional group type [33]. They showed that, contrary to the widespread view that membrane performance depends mainly on the CO_2 uptake of the filler, the permeability dependence is more complex. They suggest that isosteric heats of adsorption are a better indicator of membrane performance but conclude that there is a need for more fundamental understanding of the relationship between MOF filler properties and membrane performance.

Other studies on ZIFs have systematically examined the impact of changing a single filler characteristic on membrane performance. A comparative study of PEBAX-based membranes containing the isostructural ZIF-67 and ZIF-8, differing in metal cation (Zn^{2+} for ZIF-8, and Co^{2+} for ZIF-67), indicated the ZIF-67-based MMM generally outperformed its ZIF-8 counterpart [34]. Also, an isostructural series of ZIFs with the **gme** topology (including ZIF-68, ZIF-69, and ZIF-78) has been investigated in MMM applications; however, the particle size of the MOF fillers was not the same [35] and other work has shown that particle size can have an important effect on MMM performance, for example due to polymer/ZIF interface effects leading to differences in dispersion and agglomeration behaviour [13,36]. Table S1 summarises the literature comparisons of different ZIFs under similar conditions.

Most studies, however, consider the effect of adding a single type of ZIF at different loadings to a polymer and investigate the properties of the resultant MMMs for the permeation of a range of pure or mixed gases under specific conditions. Since membrane preparation and measurement conditions in different laboratories can be different, direct comparison of different studies to evaluate the effect of ZIF structure type can be difficult. Given the relative paucity of systematic investigation of the influence of structure and functionality of ZIFs of similar particle size when used as fillers in membrane-based CO_2/N_2 separation, we aimed to compare ZIFs with similar particle size as fillers within MMMs. We chose to examine ZIFs with the cubic **sod** and **rho** topologies, and the rhombohedrally-distorted **sod** topology, to separately determine the effect of ZIF structure and composition. Fig. 1 illustrates schematically the relationships of ZIF-94, ZIF-7/COK-17, and ZIF-11/ZIF-71 to ZIF-8, ZIF-7, and ZIF-11, respectively, that are relevant to our work.

Our starting structure types for consideration were the well-studied ZIF-7 and ZIF-8 **sod** types. ZIF-7 offers a more restricted pore space than ZIF-8, due to its bulkier benzimidazole linkers within the same topology, resulting in higher interaction with guest molecules (ca. 28 kJ mol^{-1} vs. 17 kJ mol^{-1} for CO_2) [37] but lower diffusivity. ZIF-8 has a larger pore size (3.4 Å) and cavity diameter (10.9 Å) compared to ZIF-7 (pore size 3.2 Å, cavity diameter 4.9 Å), enabling faster gas diffusion (self-diffusivity of CO_2 is 1.2×10^{-5} cm^2 s^{-1} in ZIF-8 vs. 4×10^{-7} cm^2 s^{-1} in ZIF-7) [37].

ZIF-7 transforms from a 'narrow-pore' form to a 'wide-pore' form upon gas adsorption, typically at 0.5 bar for CO_2 at 298 K [27]. This is expected to have a negative effect on membrane performance, degrading the polymer-filler interface [20] so we chose instead to include in this study a hybrid ZIF, intermediate between ZIF-7 and the isostructural COK-17 (zinc 4,5-dichloroimidazolate, $Zn(dcIm)_2$), which we recently reported [38]. This exhibits rigidity during CO_2 adsorption, with a high CO_2 uptake at 1 bar, similar to that COK-17 [39]. The crystal size of

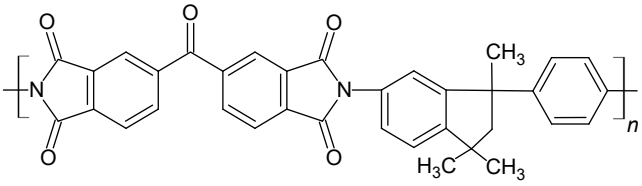

Scheme 1. Matrimid® chemical structure.

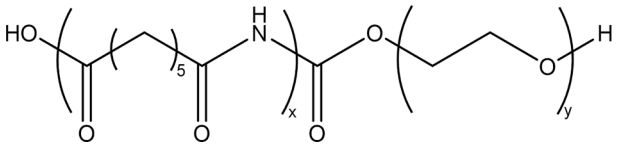

Scheme 2. PEBAX MH1657 chemical structure (x = 40, y = 60).

COK-17 (ca. 3 μm) is too large to be embedded easily into a polymeric matrix, and synthesis of COK-17 nanocrystals remains a challenge [39]. Using methanol as a solvent, $Zn(dcIm)_2$ can be directed into the more open **rho** structure, as ZIF-71 ($Zn(dcIm)_2$). A hybrid ZIF-11/ZIF-71 with the **rho** structure and the same $Zn(BzIm,dcIm)_2$ composition as the rhombohedral **sod** ZIF-7/COK-17 hybrid [38] was also included in the study to directly compare the effect of topology type.

ZIF-8 is known to possess high diffusivity, but relatively low uptake at low pressures. Additionally, the methylimidazole groups are known to exhibit linker swing, which causes a significant loss in membrane selectivity [40]. To increase strength of CO_2 interaction, and improve molecular sieving, we included ZIF-94 in our selection as a direct comparison with ZIF-8, having the same topology type but different composition. The linker in ZIF-94 is 4-methyl-5-imidazolecarboxaldehyde (AmeIm) and the presence of aldehyde groups leads to a strong improvement in CO_2 adsorption uptake compared to ZIF-8 (2.0 mmol g^{-1} vs. 0.74 mmol g^{-1} at 298 K at 1 bar) and enhances the framework rigidity [41].

Our choice of ZIFs therefore enables direct comparison of (i) ZIFs with different linkers in the same structure (ZIF-94 vs. ZIF-8, both **sod**) and (ii) ZIFs with the same composition ($Zn(dcIm,BzIm)_2$) but with different (**sod** or **rho**) topologies (ZIF-7/COK-17 vs. ZIF-11/ZIF-71). More generally, it enables a consideration of the effect of both strength of CO_2 interaction and topology type on the MMM performance.

Two commonly used polymeric materials in MMMs preparation were investigated in these studies, PEBAX MH1657 and Matrimid®5218 [19,26,42,43]. Both display high CO_2 permselectivity in CO_2/non-polar gas separations (such as CO_2/CH_4 or CO_2/N_2) due to the presence of polar segments. However, owing to their different chemical composition (Schemes 1 and 2), PEBAX, containing soft polyethylene oxide chains, shows rubbery properties while Matrimid is a type of polyimide that displays glassy properties [44,45]. Therefore we established the detailed performance of the two most strongly adsorbing ZIFs as fillers in these two polymer types before going on to compare the four selected ZIFs at 12 wt% in PEBAX MH165.

2. Materials and Methods

2.1. Materials

Matrimid®5218 and PEBAX MH1657 were supplied by Huntsman and Arkema, respectively. Matrimid®5218 is a glassy polyimide with the molecular weight of 44000 g mol^{-1} [46]. PEBAX MH1657 is a copolymer composed of 40 wt% polyamide (PA) and 60 wt% polyethylene oxide (PEO). The density of PEBAX MH1657 is 1.14 g cm^{-3}.

The grade 1657 was used due to the enhanced CO_2/N_2 separation performance reported in the literature compared to other commercial grades (such as 2533, 3533) [45].

All ZIF materials were synthesised in our laboratory using one of two types of zinc salts: zinc acetate dihydrate (Sigma-Aldrich, ≥ 99 %) or zinc nitrate hexahydrate (Alfa Aesar, 98 %). The organic linkers were 2-methylimidazole (Sigma-Aldrich, ≥ 99 %, MeIm), 4-methyl-5-imidazolecarboxaldehyde (Fluorochem, 97 %, AmeIm), benzimidazole (Alfa Aesar, 99 %, BzIm), 4,5-dichloroimidazole (Fluka, 98 %, dcIm). Methanol (99.9 %), tetrahydrofuran (99.9 %, THF), dimethylformamide (Acros Organics, 99 %, DMF), dichloromethane (Sigma-Aldrich, ≥ 99.9 %, CH_2Cl_2), ethanol (Sigma-Aldrich, ≥ 99.9 %) and deionised water were used as solvents without any purification.

2.2. ZIF synthesis

2.2.1. ZIF-8

ZIF-8 nanoparticles were synthesized according to the method of Torad et al. [47] A solution was prepared by dissolving 6 mmol Zn $(CH_3COO)_2{\cdot}2H_2O$ and 24 mmol MeIm in 200 mL methanol. The mixture was stirred for 5 min and then aged at room temperature for 24 h. The ZIF-8 crystals were collected by centrifugation at 14500 rpm and then washed with methanol three times before drying at 343 K.

2.2.2. ZIF-94

ZIF-94 synthesis was according to the protocol from Etxeberria-Benavides et al. [48]. ZIF-94 nanoparticles were prepared by dissolving 2 mmol $Zn(CH_3COO)_2{\cdot}2H_2O$ in 20 mL methanol and 4 mmol AmeIm linker in 50 mL tetrahydrofuran. The zinc acetate solution was added into linker solution, well-mixed, and vigorously stirred for 60 min at room temperature. ZIF products were collected by centrifugation at 14500 rpm and washed with methanol three times before drying at 343 K.

2.2.3. ZIF-7/COK-17

ZIF-7/COK-17 synthesis followed the protocol from Jia et al. [38]. 2 mmol $Zn(NO_3)_2$ $6H_2O$ were dissolved in 20 mL DMF, and (8–*x*) mmol of BzIm and *x* mmol dcIm were dissolved in 30 mL DMF. Both solutions were stirred at 393 K for 30 min and then cooled to room temperature before the salt solution was added to the linker mixture and stirred for another 2 h. The product was collected by centrifugation at 14500 rpm, and then washed with DMF three times. As discussed in [38], hybrid ZIF-7/COK-17 with 45 mol% dcIm outperformed other ZIFs in the ZIF-7/COK-17 series, thus, in this work, we only used ZIF-7/COK-17 with 45 mol% of dcIm.

2.2.4. ZIF-11/ZIF-71

The synthesis of **rho** structure ZIF-11/ZIF-71 followed the procedure for ZIF-7/COK-17 [38]. The only difference is using methanol as the solvent here. The product was washed with fresh methanol and dried at 343 K.

2.3. Membrane preparation

For the preparation of MMMs, we followed the widely-used process, described in several references [49–51]. In our previous work [52], we studied the optimal conditions for fabricating MMMs based on PEBAX and ZIF-8, and we followed the same procedure here.

Preparation of Matrimid®-based mixed matrix membranes

Matrimid®5218 was dried overnight at 100 °C under vacuum. 0.5 g dried polymer was dissolved in 8 g dichloromethane (CH_2Cl_2) and stirred for 1 h at room temperature. In the meantime, ZIF particles were added according to the desired loadings [0.03 g (5 %), 0.05 g (8 %), 0.07 g (12 %), 0.12 g (20 %)] and suspended in CH_2Cl_2 (2 g) by ultrasonication. Then, the two solutions were combined, stirred overnight at ambient temperature and sonicated for 10 min before casting. The resulting solution was poured into a 5 cm radius glass petri dish. The membrane was allowed to form by slow solvent evaporation for 24–36 h in a fume cupboard.

Preparation of PEBAX-based mixed matrix membranes

0.75 g PEBAX MH1657 was dissolved in a water/ethanol mixture (3.5 g/7.9 g) at 353 K under reflux for 3 h. In the meantime, ZIF crystals were added according to the loading ratios [0.04 g (5 %), 0.1 g (12 %), 0.2 g (20 %)] and suspended in water/ethanol mixture (0.5 g/1 g, 1 g/2 g, 2 g/4 g, respectively) by ultra-sonication. Then, the two solutions were combined and sonicated for 1 h before casting. The resulting solution was poured onto a glass plate and cast by the doctor blade method with a gap of 70 μm. Then, the membrane was covered with a box that had holes drilled in its top and allowed to dry for 36 h at ambient temperature

ZIF loading ratio in MMMs was calculated:

$$w_{ZIF} = \frac{W_{ZIF}}{W_{ZIF} + W_{polymer}} \tag{1}$$

As a reference, membranes based on the neat polymers were prepared by an identical procedure. The thickness of all membranes was around 30–50 μm, according to averaged measurements performed with a digital micrometer (Mitutoyo) at different locations on each membrane.

2.4. ZIF material characterization

The crystalline structure of the as-synthesized and activated materials was determined by powder X-ray diffraction (PXRD) on a Stoe STADIP diffractometer (Cu $K_{\alpha1}$ X-radiation, $\lambda = 1.54056$ Å, 2θ range 3 – 40°). Samples were activated by heating the sample in a tube furnace under flowing nitrogen. The composition of hybrid ZIFs were analysed by solution-state Nuclear Magnetic Resonance (NMR) spectroscopy on a Bruker AVII 400. The samples were dissolved by deuterated dimethyl sulfoxide (DMSO) with addition of concentrated HCl (37 %) to aid dissolution. The morphology of ZIF nanoparticles was examined using scanning electron microscopy (SEM) on a JSM-IT800 instrument. Thermogravimetric analysis (TGA) was run on a Stanton Redcroft STA-780 with a heating rate of 5 K min^{-1}. N_2 adsorption isotherms were measured volumetrically using a Micrometrics ASAP 2020 Gas Adsorption Analyzer at 77 K. Before measurement, ZIF samples were activated in flowing N_2 at 453 K for 10 h. The activated samples were then put under vacuum and heated to the same temperature for 8 h. High-pressure CO_2 and N_2 adsorption isotherms at 298 K were measured using a Hiden Intelligent Gravimetric Analyzer (IGA). As for the N_2 adsorption measurement, the analysed sample was activated at 453 K for 10 h prior to loading into the IGA; the samples were subsequently heated under vacuum at 453 K for 10 h. The mass change was recorded in each adsorption/desorption step, and each step continued until the mass achieved 98 % of the asymptotic equilibrium value or for 90 min, whichever was the earlier.

Heat of adsorption was determined by the Clausius-Clapeyron equation as shown below under certain pressure (*p*) and temperature (*T*) [53]:

$$\frac{dlnp}{dT} = \frac{\Delta H_{ads}(n)}{RT^2} \tag{2}$$

where ΔH_{ads} is enthalpy of adsorption in kJ mol^{-1} for a given gas loading (represented as *n*), and R is the gas constant (equal to 8.314 J K^{-1} mol^{-1}). By integrating E2, the relationship between pressure and temperature can be obtained:

$$lnp = -\frac{\Delta H_{ads}(n)}{R}\frac{1}{T} + C \tag{3}$$

where *C* is the constant.

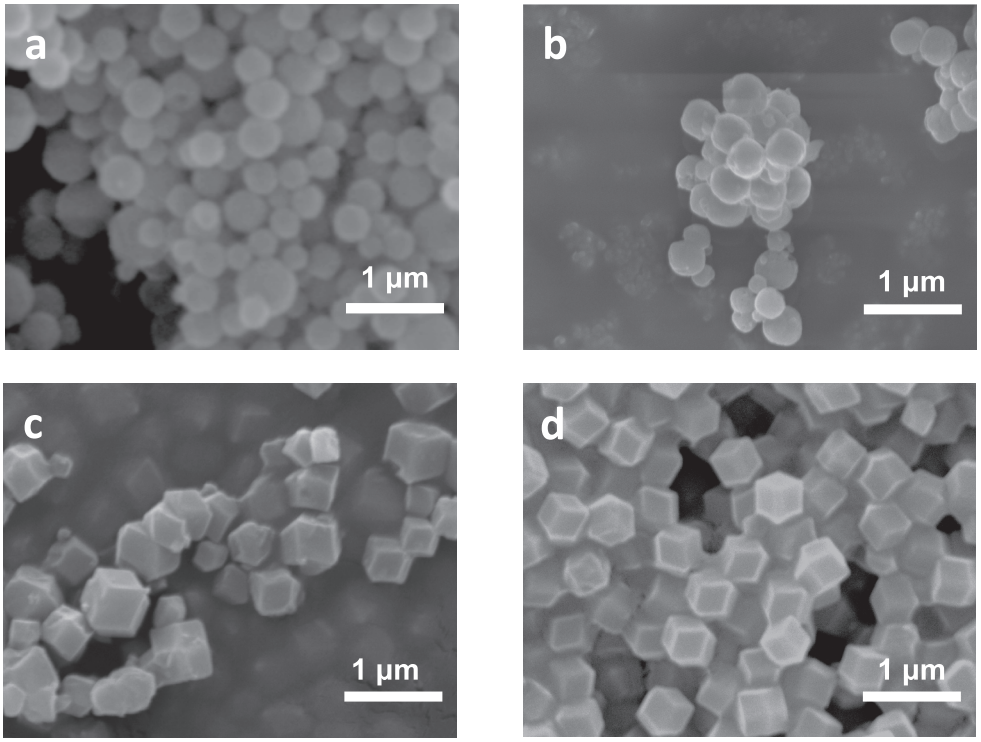

Fig. 2. SEM images of (a) ZIF-7/COK-17, (b) ZIF-94, (c) **rho** ZIF-11/ZIF-71, and (d) ZIF-8.

To determine the relationship between uptake and gas pressure, we applied the Freundlich-Langmuir isotherm equation, which can be expressed as:

$$n = \frac{a \cdot b \cdot p^c}{1 + b \cdot p^c} \tag{4}$$

where a is the maximum loading characterised in mmol g^{-1}, b represents the affinity constant, and c is the heterogeneity exponent. The isotherm expression can be determined by conducting CO_2 adsorption at different temperatures.

Due to the heterogeneity of hybrid ZIF-7/COK-17, the dual-site Freundlich-Langmuir isotherm was applied for a more accurate description, which can be expressed by:

$$n = \frac{a \cdot b \cdot p^c}{1 + b \cdot p^c} + \frac{a_1 \cdot b_1 \cdot p^{c_1}}{1 + b_1 \cdot p^{c_1}} \tag{5}$$

where a_1, b_1 and c_1 are used to interpret the adsorptive process for the second type of sites.

2.5. MMM characterization

The crystalline structure of MMMs was investigated by PXRD in flat plate geometry, on a PANalytical Empyrean diffractometer with Cu $K_{\alpha 1}$ radiation and an X'celerator RTMS detector over a 2θ range of 3 – 40°. To ensure the surface was flat, the tested membrane was attached with Vaseline. The thermal behaviour of MMMs was measured by a Netzsch Jupiter STA449 Thermogravimetric Analyzer with a heating rate of 10 K min^{-1}. The membranes were examined with a JEOL JSM-IT100 scanning electron microscope operating at 10 kV. Before SEM analysis, the samples were fractured in liquid nitrogen and then sputter-coated with a layer of 12 nm gold to give them a conductive surface.

2.6. Gas permeation measurements

Single gas permeation measurements were carried out using a custom-built constant volume-variable pressure apparatus using pure N_2 and CO_2 at 1.2 bar and 293 K (Scheme S1). The permeability is obtained from the evolution of pressure of the downstream side. For N_2, the permeation rates are low, so unavoidable contributions of small leak rates in the experimental system can introduce some systematic errors. The permeability coefficient, P, was determined from the slope of the pressure versus time curve under the steady-state condition:

$$P = \frac{l}{A} \frac{V_{down}}{P_{up} RT} \left[\left(\frac{dP_{down}}{dt} \right)_{ss} \right] \tag{6}$$

where l is the membrane thickness [m], A is the membrane area [m^2], V_{down} is the downstream volume [m^3], P_{up} is the upstream pressure [Pa], P_{down} is the downstream pressure [Pa], T is the temperature recorded during analysis [K] and R is the gas constant [J K^{-1} mol^{-1}]. This will give the permeability in SI units [mol m m^{-2} s^{-1} Pa^{-1}]. To convert to Barrer, the permeability in SI units was multiplied by 2.9×10^{15}.

The time lag, θ, was used to determine the diffusivity coefficient D:

$$D = \frac{l^2}{6\theta} \tag{7}$$

The solubility coefficient, S, for the gas in the polymer was evaluated indirectly, assuming the validity of the solution-diffusion mechanism:

$$S = \frac{P}{D} \tag{8}$$

The ideal selectivity between two gas species i and j is the ratio of the two single gas permeabilities:

$$\alpha_{ij} = \frac{P_i}{P_j} \tag{9}$$

3. Results and discussion

3.1. Preparation and characterisation of ZIF materials

ZIF-7/COK-17 and ZIF-94 are functionalised materials related to ZIF-7 and ZIF-8, respectively. The synthesis for both types of ZIFs is fast and

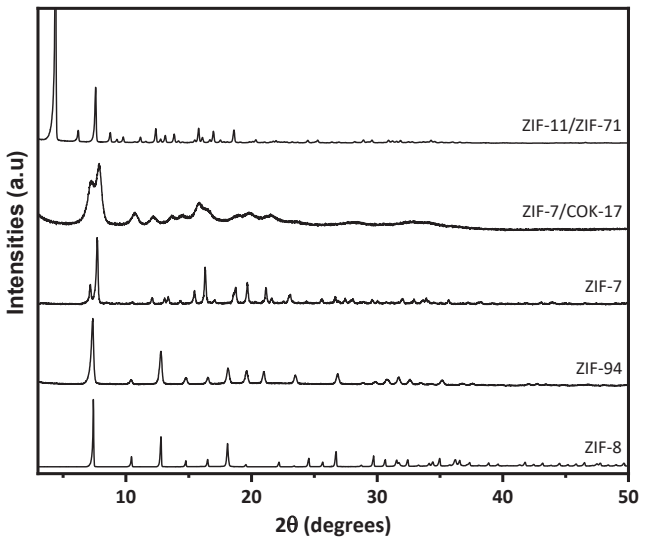

Fig. 3. PXRD patterns of ZIF materials studied in this work (Cu Kα$_1$, λ= 1.54056 Å). All patterns scaled to the most intense peak except ZIF-11/ZIF-71, scaled on 0.5× most intense peak. Data on ZIF hybrids from reference [38].

Table 1
BET surface areas and accessible pore volumes of ZIFs, from N_2 adsorption at 77 K.

MOF materials	ZIF-7	ZIF-8	ZIF-7/ COK-17	ZIF-94	ZIF-11/71
BET surface area ($m^2\ g^{-1}$)	311	1261	351	390	751
Accessible pore volume ($cm^3\ g^{-1}$ at P/Po = 0.2)	0.14	0.63	0.18	0.19	0.38

yields nanocrystals (ca. 300 to 400 nm, Fig. 2a and b). Nanocrystals of ZIF-8 and **rho** ZIF-11/ZIF-71 of similar sizes were also prepared, to enable comparison (Fig. 2c and 2d). To eliminate the effect of chemical composition on hybrid MOF properties, the linker ratios in ZIF-11/ZIF-71 and ZIF-7/COK-17 were controlled to be identical, as measured by ^{1}H NMR (Fig. S1).

The samples of ZIF-7/COK-17 and ZIF-94 were confirmed to be closely related to those of ZIF-7 and ZIF-8 by PXRD (Fig. 3). ZIF-94 exhibits cubic symmetry like ZIF-8, and ZIF-7/COK-17 shows rhombohedral symmetry characteristic of the open form of ZIF-7. The structure of hybrid ZIF-11/ZIF-71 displays the **rho** topology.

The porosity of ZIFs with pore sizes above ca. 3 Å is assessed by N_2 adsorption at 77 K (Table 1). Their accessible volume and effective surface area impact strongly upon gas transport, and as a general principle, a larger accessible volume corresponds to higher gas diffusivity [54,55]. The isotherms (plotted vs. relative pressure and vs. a logarithmic pressure scale) are given for all ZIFs in Fig. 4. The N_2 uptakes of ZIF-7, ZIF-8 and ZIF-94 are consistent with the results from previous studies [56].

ZIF-8 has the highest N_2 uptake capacity and BET surface area of the materials under study. The two-step feature in the isotherm as shown by the logarithmic scale of relative pressure (Fig. 4b) is a result of a phase transition within ZIF-8, involving linker swing to facilitate adsorbate accommodation and subsequent adsorbate repacking within ZIF-8 cage [57]. Substitution with AmeIm gives ZIF-94 a more rigid structure displaying a Type I isotherm. The lower specific uptake results from the aldehyde groups projecting into the pore space and adding additional mass. ZIF-7, for which the 77 K N_2 isotherm is shown here for comparison, also undergoes a phase transition, its empty phase characterised by narrow pores that render it unable to adsorb N_2 at low partial pressure. After inclusion of dcIm, in ZIF-7/COK-17, there is a Type I isotherm (no phase transition) and a slightly increased BET surface area compared to the open form of ZIF-7 (from 310 $m^2\ g^{-1}$ to 350 $m^2\ g^{-1}$). The partial substitution of the smaller linker is responsible for higher surface area and also imparts structural rigidity. The **rho** ZIF-11/ZIF-71 hybrid shows a higher N_2 uptake at 77 K compared to its compositional **sod** topology counterpart (ZIF-7/COK-17), as a result of its more open structure (Fig. 1). The specific uptake of ZIF-11/ZIF-71 is higher than that reported for ZIF-11 (180 cm^3 (STP) g^{-1}) [58], which is attributed to its less bulky dcIm linkers.

Membrane selectivity is closely linked to the affinity of the materials towards guest molecules, which can be determined by examining the gas adsorption isotherms at ambient temperature. Therefore, in this study, the CO_2 and N_2 uptake isotherms of the materials under investigation were evaluated gravimetrically at 298 K using an IGA instrument (Fig. 5 and Table 2). For CO_2 adsorption at 298 K (Fig. 5), ZIF-94 and ZIF-7/COK-17 display strongly convex Type I isotherms that indicate strong interactions with CO_2 that lead to uptakes of ca. 2 mmol g^{-1} at 1 bar. By contrast, ZIF-8 and ZIF-11/ZIF-71 show low uptakes below 2 bar (<1 mmol g^{-1}) that suggest weak affinity to CO_2 molecules, but a steady increase of CO_2 uptake at pressures up to 10 bar due to their large accessible volumes being capable of accommodating CO_2 molecules [59]. For the conditions of membrane testing (293 K and 1.2 bar), it is unlikely for the gate opening to occur in ZIF-8, because the loadings are relatively low (only one or two CO_2 molecules occupying each cage) [59,60]. In terms of the adsorption of N_2 in the ZIFs (the membrane

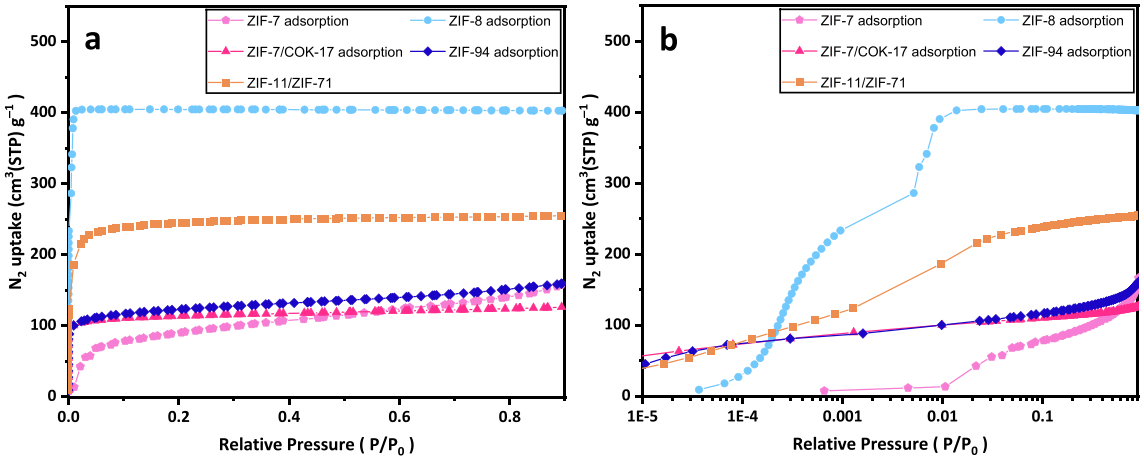

Fig. 4. N_2 adsorption isotherms at 77 K of ZIF-7 (pentagon), ZIF-8 (circle), ZIF-7/COK-17 (triangle), ZIF-94 (rhombus), and ZIF-11/ZIF-71 (rectangle) given with (a) a linear pressure scale and (b) a logarithmic pressure scale. Data on hybrid ZIFs from reference [38].

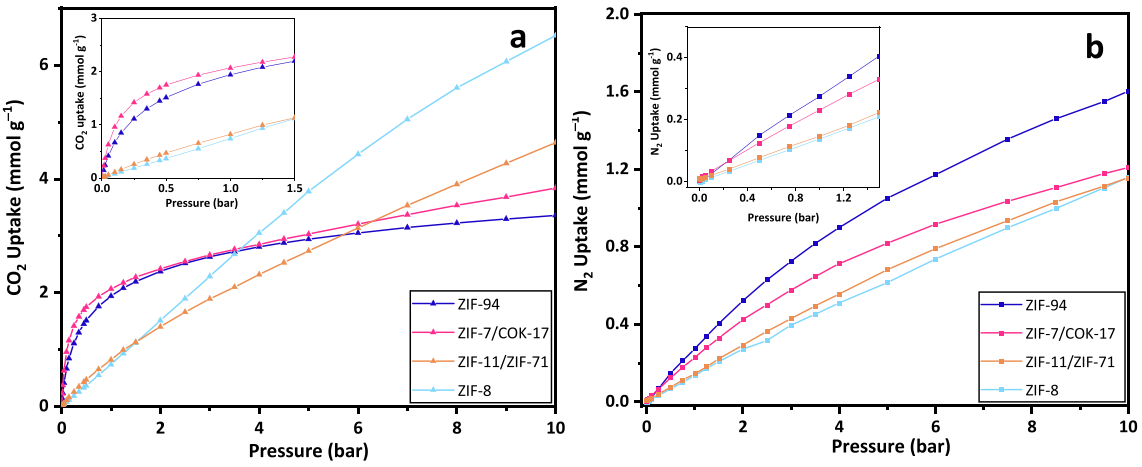

Fig. 5. (a) CO_2 adsorption isotherms (triangles) at 298 K; (b) N_2 adsorption isotherms (squares) at 298 K, in each case for the ZIFs of this study. Data on ZIF hybrids from reference [38].

Table 2
CO_2 and N_2 uptakes at 1.25 bar at 298 K for ZIF materials and their heat of adsorption for CO_2.

ZIF materials	ZIF-8	ZIF-94	ZIF-7/COK-17	ZIF-11/ZIF-71
CO_2 uptake (mmol g^{-1})	0.94	2.08	2.11	0.99
N_2 uptake (mmol g^{-1})	0.17	0.34	0.28	0.18
CO_2/N_2 uptake ratio	5.5	6.1	7.5	5.5
Heat of CO_2 adsorption / kJ mol^{-1}	17[61] (0.4–2.2 mmol g^{-1})	35.3–24.1 (0.4–2.2 mmol g^{-1})	35.3–22.4 (0.4–2.2 mmol g^{-1})	14.6–9.4 (0.4–0.9 mmol g^{-1})

selectivity of CO_2 to N_2 should be high for the application of interest), it was expected that lower N_2 uptakes could lead to low MMM N_2 solubility, and potentially higher selectivity. The isotherms are given in Fig. 5b and the uptakes at 1.25 bar are given in Table 2 along with the ratio of CO_2 to N_2 uptakes at 1.25 bar, which could be an important parameter in establishing membrane selectivity. ZIF-94 displays the highest N_2 uptake (0.34 mmol g^{-1} at 1.25 bar) which agrees well with previous results [56]. By contrast, the isostructural ZIF-8 has the lowest N_2 uptake (0.17 mmol g^{-1} at 1.25 bar). The origin of this significant difference in N_2 uptake is from asymmetric functionalisation of ZIF-94 contributing to stronger electrostatic interactions with N_2 (quadrupolar moment in N_2 (15.2×10^{-27} esu^{-1} cm^{-1})) [61,62]. A slightly lower N_2 uptake is observed in ZIF-7/COK-17 (0.28 mmol g^{-1} at 1.25 bar) compared to ZIF-94, but this is still higher than observed for its **rho** compositional counterpart (0.18 mmol g^{-1} at 1.25 bar). This can be rationalised by the more confined volume contributing to higher adsorption energy, which is commonly seen in **sod** and **rho** ZIFs of the same compositions [41]. Moreover, the N_2 uptake in ZIF-7/COK-17 is comparable to COK-17 [63], suggesting the intrinsic rhombohedral **sod** cage is a major contributor for high N_2 uptake. The CO_2/N_2 uptakes at 1.25 bar decrease in the order: ZIF-7/COK-17 > ZIF-94 > ZIF-8 = ZIF-11/ZIF-71.

The heats of adsorption of CO_2 on ZIF-94 and ZIF-7/COK-17 are derived by measuring CO_2 uptake isotherms at different temperatures (from 288 K to 318 K with a step of 10 K, seen in Fig. S2). The adsorption isotherm of ZIF-94 is fitted by applying a single-site Freundlich-Langmuir (FL) model (Fig. 6a), while the dual-site Freundlich-Langmuir is applied to fit the adsorption isotherm of ZIF-7/COK-17 (Fig. 6b). The parameters for the Freundlich-Langmuir equations are listed in Table S2, and the preferred models are consistent with the different window sites available for these two materials. Using these fitted isotherms at different temperatures, the heats of adsorption were calculated as a function of uptake (Fig. S3,Table 2). As indicated in Fig. 6, up to 2 mmol g^{-1}, both ZIFs achieve comparable heats of adsorption and demonstrate a gradual decrease with CO_2 loading from 35 kJ mol^{-1} at 0.4 mmol to 25 kJ mol^{-1} at 2 mmol g^{-1}. Above 2 mmol g^{-1} loading of CO_2, the heat of adsorption on ZIF-94 continues to decrease gradually, while the heat of adsorption from hybrid ZIF-7/COK-17 experiences a sharp decrease to 15 kJ mol^{-1} at 2.4 mmol g^{-1}. This is related to their structure and surface chemistry: for ZIF-94, the cubic structure and single ligand composition give rise to only one type of six-membered ring serving as the adsorptive site. For ZIF-7/COK-17, the rhombohedral **sod** structure has two types of six membered rings, and the heterogeneity of pore structure is further increased due to the mixed-linker composition [64].

Additionally, the heat of adsorption of **rho** ZIF-11/ZIF-71 is determined through the analysis of its adsorption isotherms at different temperatures (Fig. S4) and plotting ln*p* vs. 1/T for different uptakes (Fig. 6d), although good fits were not obtained using the FL isotherm model. At the uptake of 0.4 mmol g^{-1}, the heat adsorption is 14 kJ mol^{-1}, which is much lower than the heat adsorption derived for ZIF-7/COK-17, and the heat decreases at higher loadings (Table 2). This underlines CO_2 adsorption favours the **sod** structure with smaller pore size [41]. For membrane application at 1.2 bar and room temperature, the corresponding gas uptakes and the relevant heats of adsorption for CO_2 are compared in Table 2. The heat adsorption of ZIF-8 quoted is from a previous study [65].

In summary, two ZIFs selected for their strong interactions with CO_2 have been synthesised in nanoparticulate form and their BET surface area and gas adsorption isotherms measured. These have been compared with those of two ZIFs of similar particle size but without strong CO_2 interactions that have been chosen to enable quantification of the effect of polar functional groups and framework topology. With regard to membrane separation, a solution-diffusion mechanism is expected to describe the process, which involves gas sorption at the upstream boundary, the diffusion of dissolved or adsorbed gas, and the desorption of gas molecules at the permeate side [66]. The rate-limiting step is the diffusion, while the quantity of sorbed gas primarily determines the gas flux. By incorporating MOF fillers, the diffusion path might be altered by making use of their porosity and modifying the membrane tortuosity, and their affinity to guest molecules will add to the total sorbed gas by the membrane. This sample set was chosen to obtain fundamental insight into the structure–property relationship of ZIF fillers to their MMM properties. Table S3 summarises the main characteristics of the ZIFs studied (including ZIF-7, ZIF-8, ZIF-94, ZIF-7/COK-17 and ZIF-11/ZIF-71). The thermal behaviour of the ZIFs has been compared between

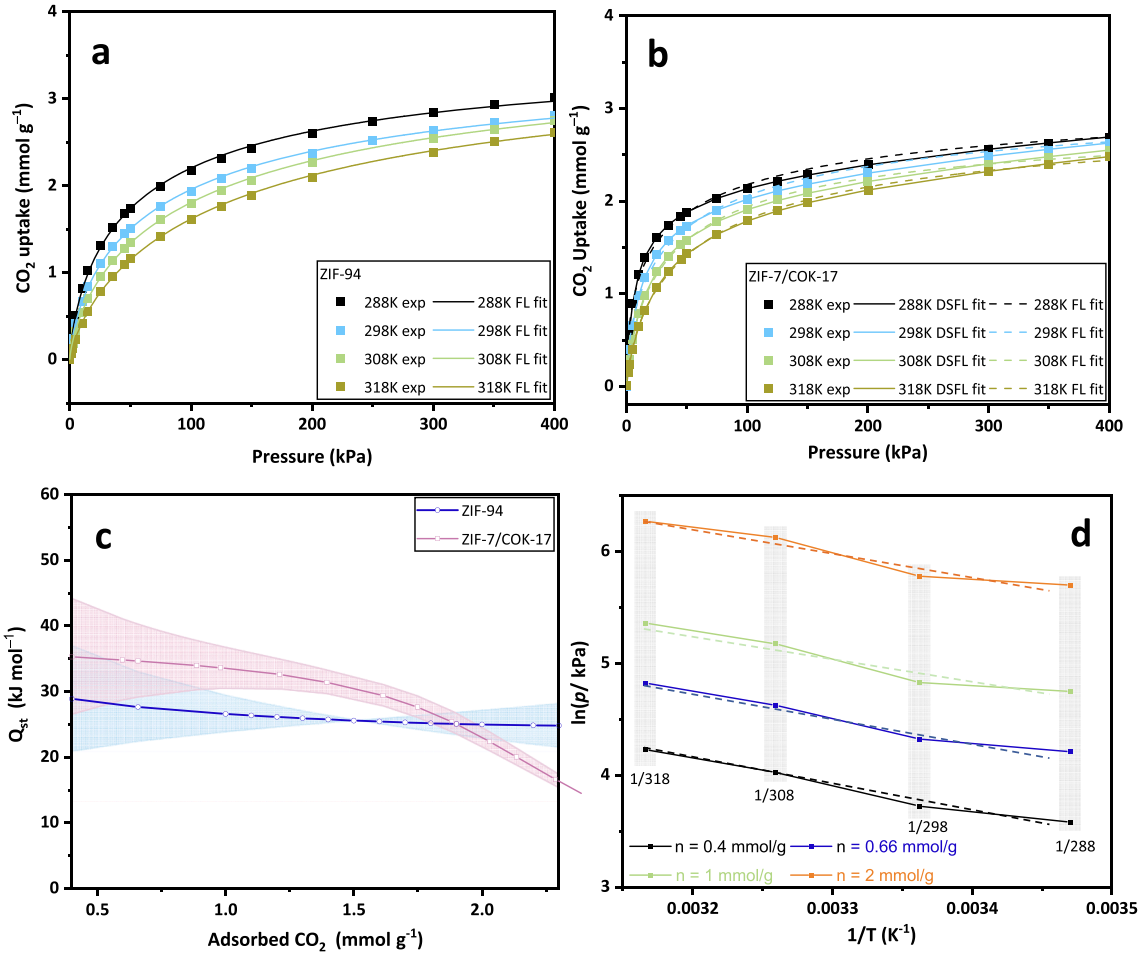

Fig. 6. The Freundlich-Langmuir fits for CO_2 adsorption isotherms in (a) ZIF-94 and (b) ZIF-7/COK-17. (c) Heat of adsorption of CO_2 for ZIF-94 and ZIF-7/COK-17 (Q_{st} from the fitted isotherms at 288 K, 298 K, 308 K and 318 K (shaded areas represent the error). (d) Isosteric ln *p* against *1/T* plot for ZIF-11/-71 (**rho**) at 288, 298, 308 and 318 K for four different loadings *n* (in mmol g^{-1}) for the determination of ΔH_{ad} (*n*).

two pairs of samples: ZIF-7 vs ZIF-7/COK-17, and ZIF-8 vs ZIF-94 (Fig. S5). In each case the ZIFs with functional groups decompose at lower temperature compared to their counterparts, which is attributed to the lower bond strengths of RC-CHO (RC represents the imidazole ring) and RC-Cl compared to RC-CH_3 and RC-Ar.

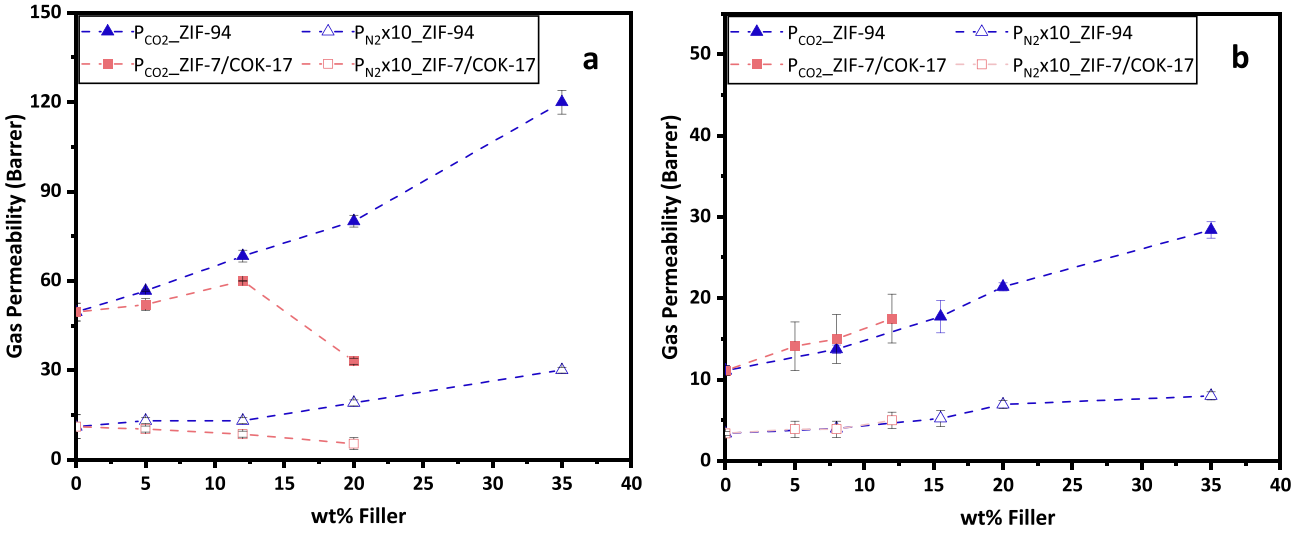

Fig. 7. CO_2 and N_2 permeability (10 × P_{N2}) for (a) PEBAX-based membranes and (b) Matrimid®-based membranes as a function of ZIF loading (ZIF-94, blue triangle and ZIF-7/COK-17, pink square. Plain marker, CO_2 permeability; empty marker, N_2 permeability). The error bar is based on the reproducibility of the experiment (2 or 3 samples tested for each point).

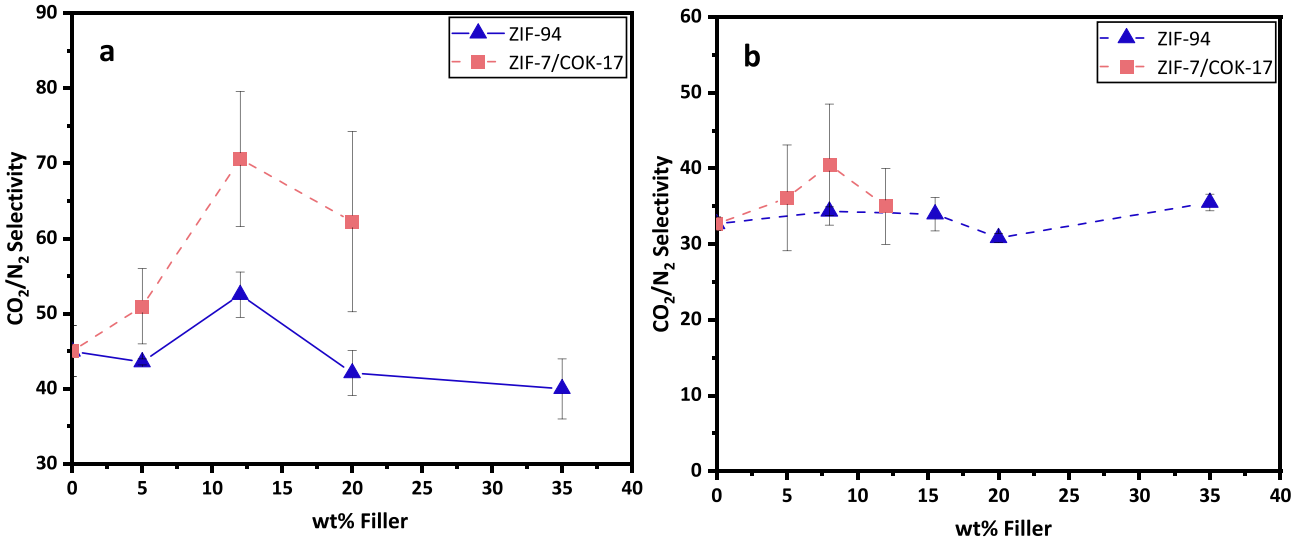

Fig. 8. CO_2/N_2 selectivity for (a) PEBAX-based membranes and (b) Matrimid-based membranes as a function of ZIF loading (ZIF-94, blue triangles; ZIF-7/COK-17, pink squares). Data on ZIF-7/COK-17 hybrid from reference [38].

3.2. Mixed matrix membrane characterisation of MMMs with ZIF-94 and ZIF-7/COK-17

The first stage was to measure the loading-dependent behaviour of MMMs containing the two ZIFs exhibiting enhanced interactions with CO_2 (i.e. ZIF-94 and ZIF-7/COK-17) within Matrimid®5218 and PEBAX 1657. The solution casting method was used to give membranes around 30 to 50 μm in thickness, as described in the Materials and Methods section. The SEM images in Figs. S6 – S9 demonstrate a good dispersion of ZIF-94 and ZIF-7/COK-17 independent of the polymers used. For the same polymer, the SEM images are very similar between the two ZIFs. As to ZIF-94, up to 35 wt%, from the surface and cross-section, no defects or agglomeration are observed, indicating that MOF particles are distributed uniformly throughout the polymer matrix for both PEBAX and

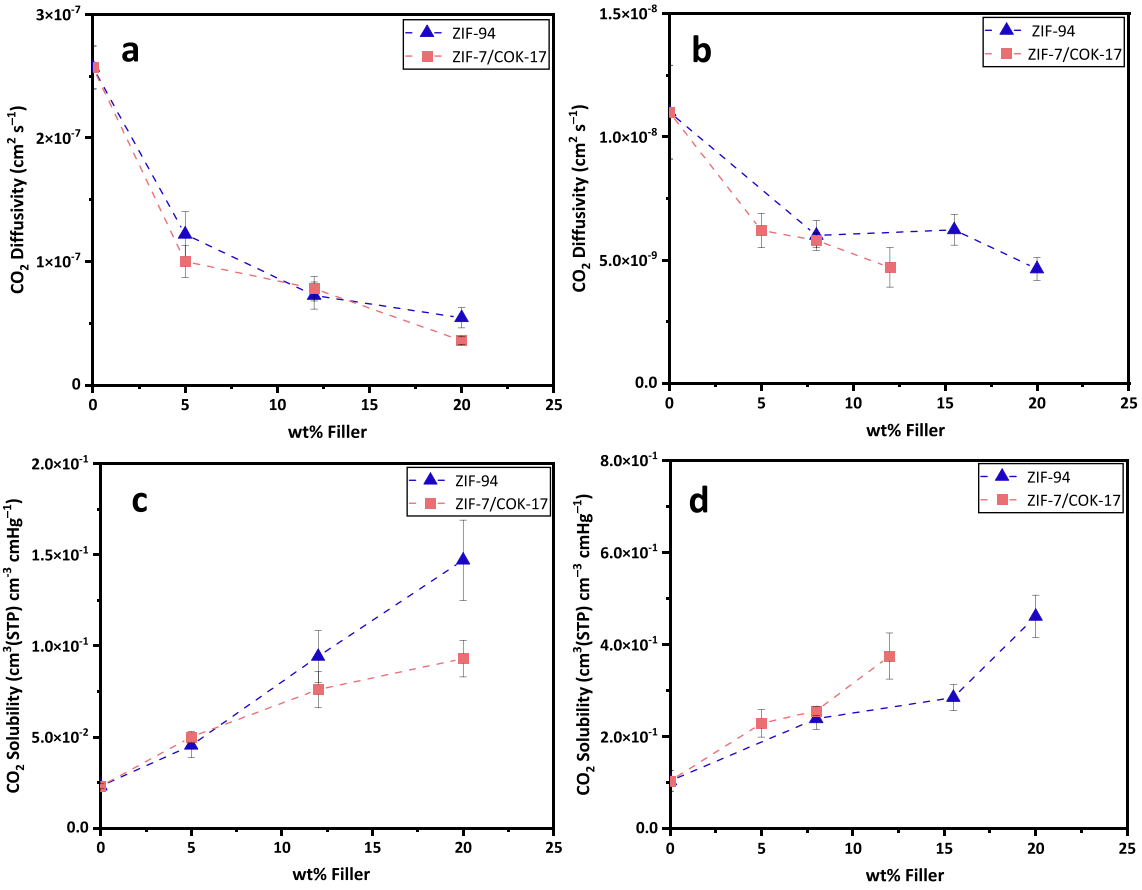

Fig. 9. CO_2 diffusivity and solubility for (a, c) PEBAX-based membranes and (b, d) Matrimid®-based membranes as a function of ZIF loading (ZIF-94, blue triangle; ZIF-7/COK-17, pink square). Data on ZIF-7/COK-17 hybrid from reference [38].

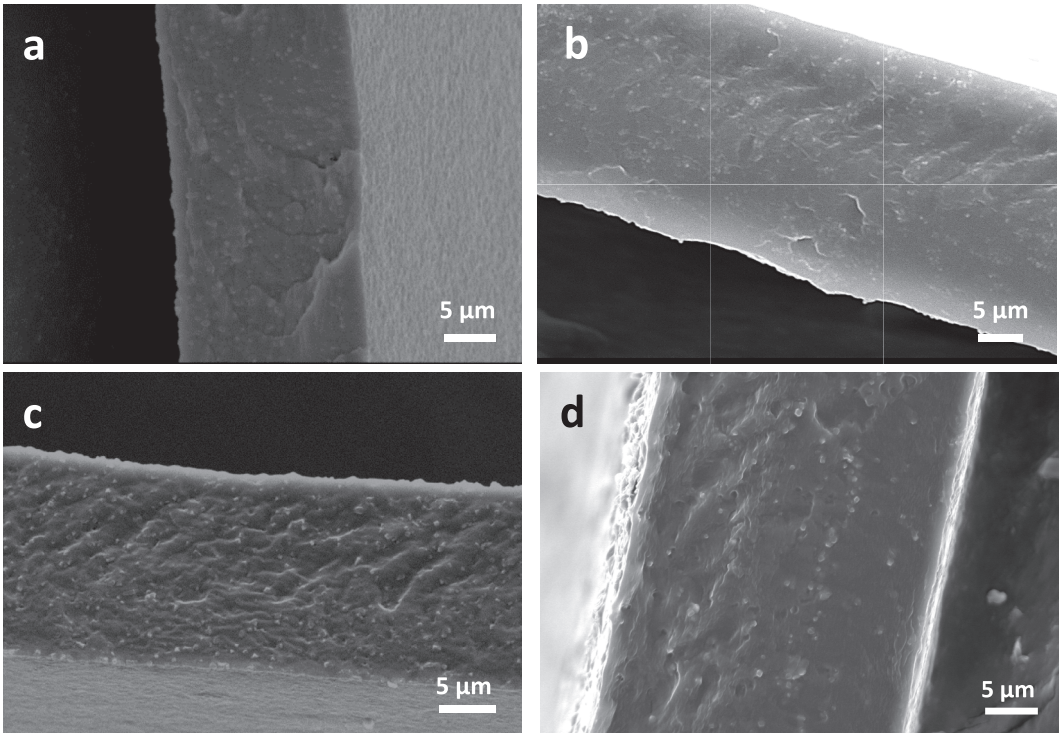

Fig. 10. SEM images of cross sections of 12 wt% ZIF in PEBAX MMMs: (a) ZIF-94, (b) ZIF-7/COK-17, (c), ZIF-8, and (d) ZIF-11/ZIF-71.

Matrimid®. However, at higher loading some defects have been noticed for the PEBAX-based MMM with the presence of pinholes (Fig. S9h). For ZIF-7/COK-17, the presence of defects appears at a lower content. As shown in Fig. S9f, agglomerations appear at 20 wt%.

XRD patterns of the MMMs (Fig. S10) demonstrate that the crystallinity of the ZIFs is retained after incorporation within the polymers, regardless of polymer type. TGA curves of the Matrimid® and PEBAX-based MMMs (Fig. S11) suggest that varying the ZIF-fillers has an insignificant effect on the MMMs' thermal behaviour, with all giving a slight acceleration of their decomposition. Table S3 summarises the glass transition temperatures and melting temperatures. The PEBAX displays dual melting peaks at 295 K and 490 K assigned to the melting process of polyethylene oxide (PEO) and polyamide (PA) respectively, and a glass transition temperature at about 215 K. By contrast, Matrimid® is remarkably stable even at temperature exceeding 573 K and a glass transition point appears at 582.7 K. Furthermore, the incorporation of ZIF fillers has only a very small effect on the membranes' thermal properties, raising the glass transition temperature by 2 K (PEBAX) and 10 K (Matrimid).

The permeation of pure CO_2 and N_2 gases through neat polymer membranes and the MMMs containing ZIF-94 and ZIF-7/COK-17 was evaluated at 1.2 bar absolute and 293 K. Fig. 7a and b show the CO_2 and N_2 gas permeation for MMMs based on PEBAX and Matrimid® respectively as a function of ZIF loading.

Up to 12 wt%, the CO_2 permeability follows the same trend for the two fillers in each of the polymers, with an increase in permeability with the ZIF-content. The CO_2 permeability is improved for PEBAX and Matrimid® by 38 % and 55 % respectively for ZIF-94, and by 20 % and 54 % respectively for ZIF-7/COK-17. At higher ZIF content (20 wt%), ZIF-94-based MMMs demonstrate a steady increase of CO_2 permeability with increasing ZIF content for both polymers while ZIF-7/COK-17 shows a strong decrease in the case of PEBAX and a sharp increase for Matrimid® up to 35.2 Barrer (not shown), which is attributed to the development of defects in the membrane. This contrasting behaviour can be related to the compatibility between fillers and polymers. The behaviour of ZIF-94 MMMs indicates compatibility between filler and polymer materials. In contrast, the results of ZIF-7/COK-17 at 20 wt% loading with both polymeric matrixes indicates poor compatibility as confirmed by SEM images: in the case of PEBAX, agglomeration is observed that leads to a decrease in permeability (Fig. S9e) while for Matrimid® defects can be identified explaining the unexpectedly high permeability (Fig. S7h). The maximum loading for ZIF-7/COK-17 to give high quality membranes is therefore 12 wt%.

The CO_2/N_2 selectivity (Fig. 8) was calculated by comparing permeation of the pure gases shown in Fig. 7. The CO_2/N_2 selectivity fluctuates slightly with the change of ZIF-94 loading in both PEBAX and Matrimid® polymers. The behaviour is similar for ZIF-7/COK-17 in Matrimid® but an improvement in ideal CO_2/N_2 selectivity can be observed at 12 wt% in PEBAX ($CO_2/N_2 = 69$). This is derived from the reduced permeability of N_2 of 0.85 Barrer.

To further investigate the trend in CO_2 permeability, the CO_2 diffusivity and solubility have been calculated. As the MMMs are considered to be dense membranes, the solution-diffusion mechanism can be applied, which considers the effective permeability as the product of effective solubility and effective diffusivity. Diffusivity coefficients were calculated from experimental pressure–time curves using Equation (7) in Methods while solubility coefficients are obtained from Equation (8). As shown in Fig. 9, the incorporation of ZIF induces a sharp decrease in CO_2 diffusivity, by 75 % for PEBAX-based MMM and by 80 % for Matrimid®-based MMM regardless of ZIF filler types, while the solubility increases in each case. The similar trend for both ZIF fillers can be explained by their similar, relatively low, accessible volumes and BET surface areas (Fig. 4), which is consistent with previous observations indicating that the BET surface area is a key property in determining permeability [32].

In the literature, there are contrasting reports of the trend of diffusivity variation with increased filler loading. A similar sharply decreasing trend in diffusivity with loading to those observed here is also observed for CO_2 over ZIF-300 in PEBAX at 4 bar and 295 K [31] but for ZIF-67 (the cobalt-version of ZIF-8) diffusivity has been measured to increase markedly with loading, while the solubility was observed to show only a small increase over the same range [67] and ZIF-67 and ZIF-

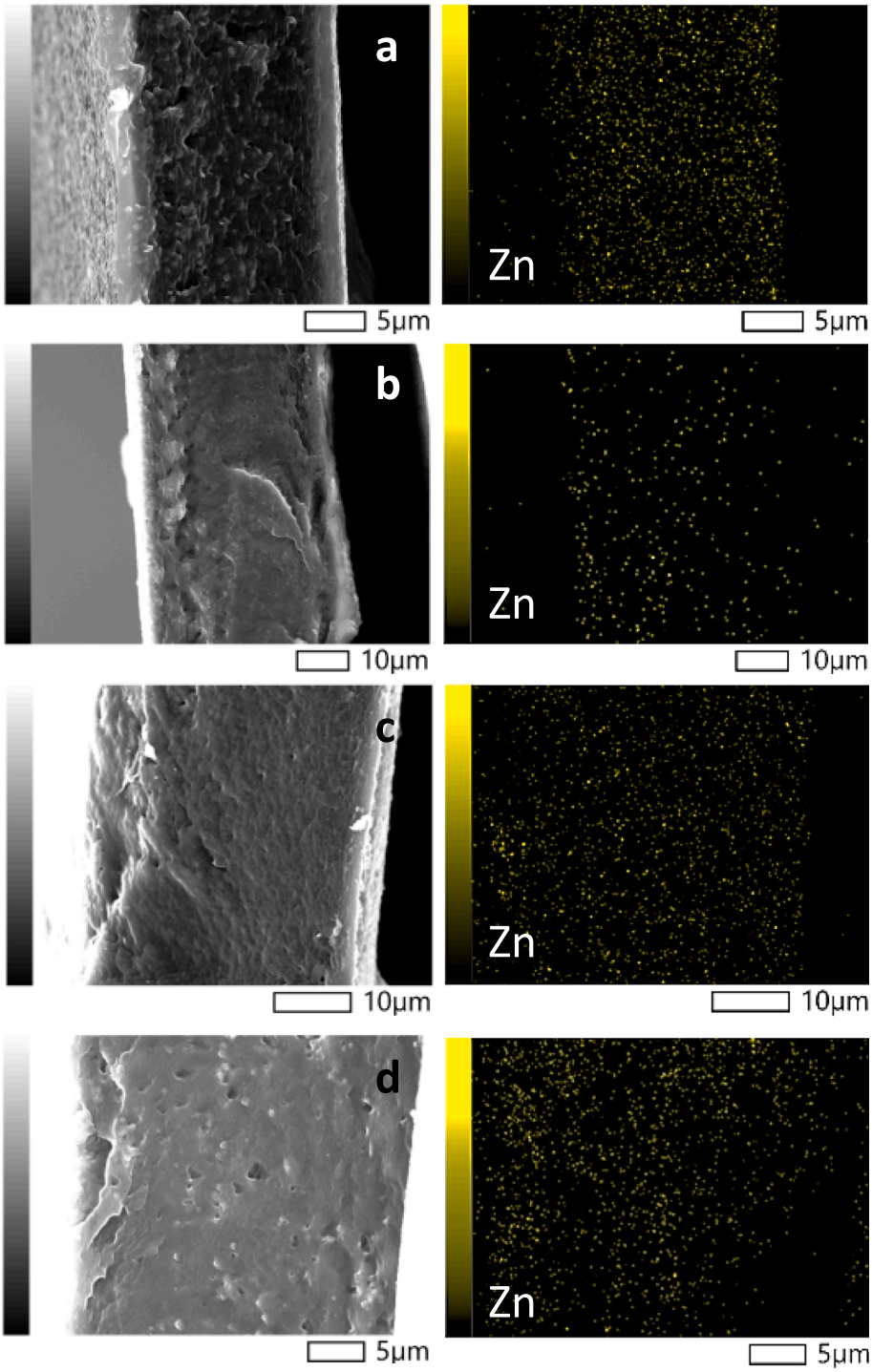

Fig. 11. Element mapping (right) of SEM cross-sections of 12 wt% ZIFs in PEBAX MMMs (left): (a) ZIF-94, (b) ZIF-7/COK-17, (c) ZIF-8 and (d) ZIF-11/ZIF-71.

8 are reported elsewhere to show increases of diffusivity with loading [34]. For the measurements here, the decrease in diffusivity compared to the pure membrane can be attributed to the interaction between fillers and polymer that constrains the mobility of polymer chain and affects the overall diffusion properties [68]. Polymer chains will tend to be rigidified with addition of fillers leading to a reduction in diffusivity. As might be expected, the addition of each ZIF to each polymer results in a steady increase in CO_2 solubility. This is explained by the high CO_2 capacity of the two ZIFs compared to the polymers themselves (Fig. 5a). This increase in membrane CO_2 solubility more than compensates for the reduction of CO_2 diffusivity, leading to the positive effect on CO_2 permeability seen in Fig. 7.

From these measurements, MMMs with 12 wt% loading of ZIF filler in PEBAX was chosen to be used in the comparison with ZIF-8 and ZIF-11/-71, because PEBAX MMMs showed the most suitable properties overall and higher loadings of ZIF-7/COK-17 in both polymers led to unfavourable dispersion and/or defects.

3.3. Comparison of ZIF-94, ZIF-7/COK-17, ZIF-8 and ZIF-11/ZIF-71 as fillers in PEBAX under similar conditions

To understand better the effect of structural parameters of ZIF fillers

Table 3
Summary of performance of ZIF-PEBAX MMMs.

ZIF – PEBAX	ZIF-8 MMM	ZIF-94 MMM	ZIF-7/COK-17 MMM	ZIF-11/ZIF-71 MMM
ZIF loading	12 wt% in all cases			
CO_2 Permeability (Barrer)	81.8	68.3	59	61
CO_2/N_2 Selectivity	52	53	69	45.7
CO_2 diffusivity (10^{-7} cm^2 s^{-1})	1.82	0.72	0.78	1.87
CO_2 solubility (cm^3(STP) cm^{-3} $cmHg^{-1}$)	0.0452	0.094	0.076	0.033

on the permeability and selectivity of MMMs, we compared the performance of the PEBAX-based MMMs with ZIF-94 and ZIF-7/COK-17 with those incorporating the other two ZIFs prepared here: ZIF-8 and ZIF-11/ZIF-71. To eliminate the effects derived from membrane parameters, we used the same loading (12 wt%) and similar particle sizes (400 nm) (Fig. 2). The surface and cross-section of MMMs prepared with ZIF-8 and ZIF-11/ZIF-71 along with ZIF-94 and ZIF-7/COK-17 are shown in Fig. 10, demonstrating a homogeneous dispersion of all ZIF fillers at this loading level. The corresponding element maps of these MMMs are shown in Fig. 11 (cross-sections) and Fig. S12 (surfaces).

The CO_2 permeability of the four PEBAX-based MMMs is compared in Table 3 (which gives all relevant properties) and Fig. 12a. At a loading of 12 wt%, the MMMs demonstrate varying levels of enhancement in CO_2 permeability, from 20 % to 60 %, where the highest CO_2 permeability is observed for ZIF-8-based MMMs (81 Barrer). For CO_2/N_2 selectivity (Fig. 12c), the ZIF-7/COK-17-containing MMM outperforms the membranes with other fillers, which is ascribed to a significant reduction in N_2 permeability with addition of this ZIF (Fig. 12b). With the exception of ZIF-7/COK-17, incorporation of ZIF fillers results in an increase in N_2 permeability. We speculate that this is due to the uniform pore sizes in the case of ZIF-8 and ZIF-11/ZIF-71 or the strong affinity to N_2 in the case of ZIF-94. ZIF-7/COK-17 possesses narrower 6R openings, some of which are highly distorted (Fig. 1) and which may result in a decreased nitrogen permeability.

The CO_2 diffusivity and solubility calculated based on Eqs. (7) and (8) are depicted in Fig. 13a and b. Regarding gas diffusivity, all show reduced values compared to the pure PEBAX, but membranes with ZIF-8 and ZIF-11/ZIF-71 fillers display higher diffusivity values compared to those with ZIF-94 and ZIF-7/COK-17. This can be attributed to their greater accessible volumes and pore sizes, as shown by Fig. 4. In the case of the 'ZIF-8 vs ZIF-94′ comparison, the increased accessible volume and larger pore size in ZIF-8 is the result of the reduced size of the imidazolate linker (MeIm) and possibly some linker motion. Additionally, the reduced diffusivity in the membrane containing the ZIF-7/COK-17 hybrid compared to that with ZIF-8 is consistent with the reduced self-diffusivity of CO_2 in ZIF-7 (4×10^{-7} cm^2 s^{-1}) compared to that in ZIF-8 (1.2×10^{-5} cm^2 s^{-1}) as calculated by Verploegh et al. [37] In the 'ZIF-7/COK-17 vs ZIF-11/ZIF-71′ comparison, the **rho** structure ZIF-11/ZIF-71, characterised by 8 membered-rings and large *lta* cages, provides a larger available volume compared to the rhombohedrally-distorted **sod** structure ZIF-7/COK-17. As for gas solubility, the MMMs with ZIF-94 and ZIF-7/COK-17 exhibit higher values than ZIF-8 and ZIF-11/ZIF-71, consistent with the fillers' high affinity for CO_2 shown in Fig. 5. Comparing between the permeability of the cubic **sod** ZIFs, the increase in solubility of CO_2 in ZIF-94 over ZIF-8 does not compensate for the reduction in diffusivity. For the hybrid ZIFs, the increased solubility of

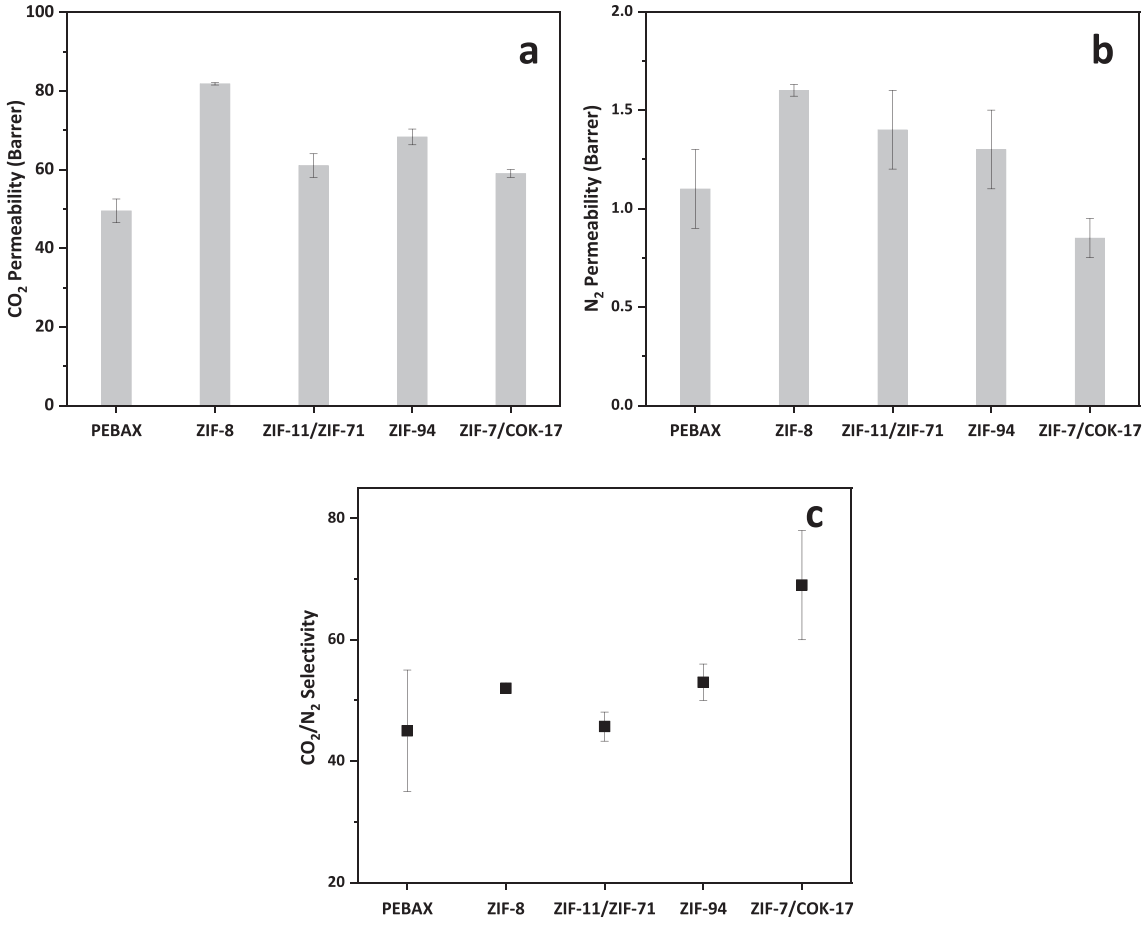

Fig. 12. (a) CO_2 permeability, (b) N_2 permeability and (c) CO_2/N_2 selectivity of 12 wt% ZIF in PEBAX MMMs, in each case compared with PEBAX membrane.

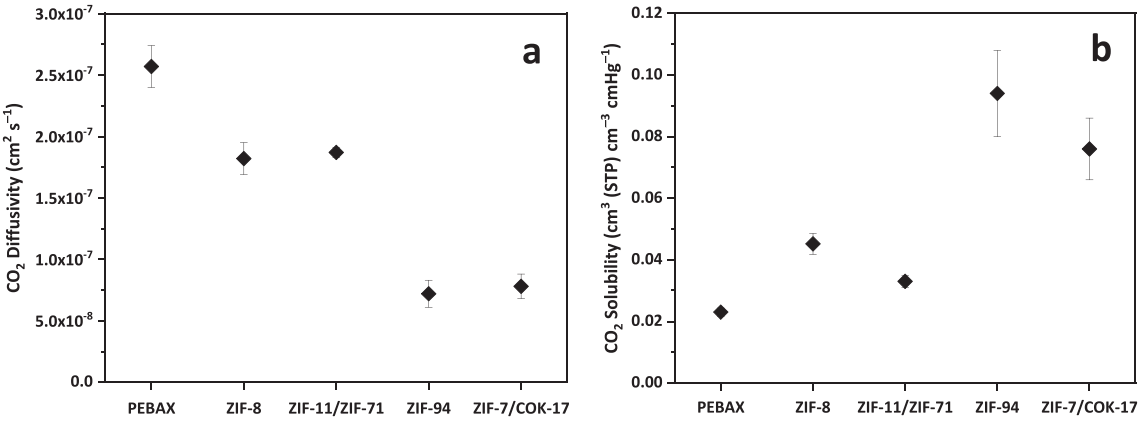

Fig. 13. (a) CO_2 diffusivity and (b) CO_2 solubility coefficients of 12 wt% ZIF in PEBAX MMMs with different ZIF fillers, compared to those of PEBAX membrane.

CO_2 in the rhombohedral **sod** structure over that in the **rho** structure is also outmatched by the reduction in diffusivity, but here the overall effect is small.

These results highlight the importance of considering both solubility and diffusivity in the choice of fillers as they have contrasting effects that tend to reduce any improvement in permeability conferred by increased solubility; the affinity of the filler for CO_2 will determine the solubility while the dimensions and connectivity of the pore openings and possibly the dynamics of linker motion will affect the diffusivity. It is their combined effect that determines the gas permeation through the membrane.

There does seem to be an effect of ZIF structure on N_2 permeability and consequently on the CO_2/N_2 selectivity, which is highest for the hybrid ZIF-7/COK-17. It may be that some molecular sieving effects on the N_2 molecule (larger than CO_2) of the distorted 6Rs in the rhombohedral **sod** ZIF are important here. However, it is not possible to determine absolute values of the N_2 diffusivity and solubility very accurately due to the larger error associated with the lower values of the N_2 permeation.

4. Conclusion

Two ZIFs that display similarly high affinities for CO_2, ZIF-94 and ZIF-7/COK-17 hybrid, have been incorporated in MMMs with a rubbery polymer (PEBAX 1657) and a glassy polymer (Matrimid®5218). ZIF-94, $Zn(AmeIm)_2$, shows good compatibility in both MMMs (up to 35 wt%), whereas ZIF-7/COK-17, $Zn(BzIm,dcIm)_2$ shows uniform dispersion only up to 12 wt%, above which defects appears (agglomeration/pin holes) within PEBAX and Matrimid®. For all systems, increased homogeneous loading significantly increases permeability for CO_2 because the increase in solubility more than compensates for the decrease in diffusivity.

For PEBAX-based MMMs, ZIF-94 and ZIF-7/COK-17 have been compared as fillers at a single loading of 12 wt% with ZIF-8 and ZIF-11/-71, two ZIFs that display much weaker CO_2 uptake at the conditions of measurement of membrane properties. This enables direct comparison of the effects of linker functionality and topology type. The CO_2 permeabilities of all MMMs are increased over that of PEBAX, and ZIF-8 loaded MMM shows the highest permeability due to its relatively high diffusivity.

In general, the conclusion is that the increased solubility in MMMs that results from enhanced uptake by those ZIFs with much greater CO_2 affinity is counteracted in terms of permeability by the greater diffusivities in those ZIFs with larger cages and without functional groups, so that MMMs with the different ZIF fillers have similar CO_2 permeabilities.

Although the N_2 permeabilities are in all cases lower and consequently measured with reduced precision, it appears that transport of the larger N_2 molecule is kinetically hindered in hybrid ZIF-7/COK-17 compared to the other ZIFs, leading to an enhancement of predicted CO_2/N_2 selectivity. This is attributed to restrictions in the size of some of its 6R windows and the more constrained space of its cages in the distorted rhombohedral **sod** topology.

CRediT authorship contribution statement

Qian Jia: Writing – original draft, Methodology, Investigation. **Elsa Lasseuguette:** Writing – review & editing, Methodology, Investigation, Formal analysis. **Maria-Chiara Ferrari:** Writing – review & editing, Supervision, Resources, Conceptualization. **Paul A. Wright:** Writing – review & editing, Supervision, Resources, Conceptualization.

Declaration of competing interest

The authors declare that they have no known competing financial interests or personal relationships that could have appeared to influence the work reported in this paper.

Acknowledgments

The authors acknowledge EPSRC Grant SynHiSel (EP/V047078/1). QJ acknowledges funding from the Chinese Scholarship Council CSC scheme from the Chinese Government (201908140117). The authors also acknowledge the EPSRC Strategic Equipment Resource Grant EP/R023751/1 for the use of the Jeol JSM–IT800 electron microscope at University of St Andrews. The raw data supporting this publication can be accessed at https://doi.org/10.17630/15eb2536-4610-4943-8edd-28361816f0c8 [69].

Appendix A. Supplementary material

Supplementary data to this article can be found online at https://doi.org/10.1016/j.seppur.2024.127584.

References

[1] B. Seoane, et al., Metal–organic framework based mixed matrix membranes: a solution for highly efficient CO_2 capture? Chem. Soc. Rev. 44 (2015) 2421–2454.
[2] R.W. Baker, Membrane technology and applications, John Wiley & Sons, 2012.
[3] A. Sabetghadam, et al., Influence of filler pore structure and polymer on the performance of MOF-based mixed-matrix membranes for CO_2 capture, Chem. – A Eur. J. 24 (2018) 7949–7956.
[4] J.D. Wind, S.M. Sirard, D.R. Paul, P.F. Green, K.P. Johnston, W.J. Koros, Carbon dioxide-induced plasticization of polyimide membranes: Pseudo-equilibrium relationships of diffusion, sorption, and swelling, Macromolecules 36 (2003) 6433–6441.
[5] J.E. Bachman, J.R. Long, Plasticization-resistant Ni_2(dobdc)/polyimide composite membranes for the removal of CO_2 from natural gas, Energy Environ. Sci. 9 (2016) 2031–2036.

[6] R.R.R. Prasad, Q. Jia, P.A. Wright, Carbon capture using metal-organic frameworks, Met. Fram. Biomed. Environ. f. 155 (2021).
[7] M. Ding, R.W. Flaig, H.L. Jiang, O.M. Yaghi, Carbon capture and conversion using metal–organic frameworks and MOF-based materials, Chem. Soc. Rev. 48 (2019) 2783–2828.
[8] M. Shan, et al., Metal- and covalent-organic framework mixed matrix membranes for CO_2 separation: A perspective on stability and scalability, J. Memb. Sci. 691 (2024) 122258.
[9] Y. Cheng, et al., Mixed matrix membranes with surface functionalized metal-organic framework sieves for efficient propylene/propane separation, Adv. Mater. 35 (2023) 2300296.
[10] Q. Qian, et al., MOF-based membranes for gas separations, Chem. Rev. 120 (2020) 8161–8266.
[11] G. Chen, et al., Zeolites and metal–organic frameworks for gas separation: the possibility of translating adsorbents into membranes, Chem. Soc. Rev. 52 (2023) 4586–4602.
[12] W. Guan, Y. Dai, C. Dong, X. Yang, Y. Xi, Zeolite imidazolate framework (ZIF)-based mixed matrix membranes for CO_2 separation: A review, J. Appl. Polym. Sci. 137 (2020) 48968.
[13] A. Imtiaz, M.H.D. Othman, A. Jilani, I.U. Khan, R. Kamaludin, O. Samuel, ZIF-filler incorporated mixed matrix membranes (MMMs) for efficient gas separation: A review, J. Environ. Chem. Eng. 10 (2022) 108541.
[14] J. Yao, H. Wang, Zeolitic imidazolate framework composite membranes and thin films: synthesis and applications, Chem. Soc. Rev. 43 (2014) 4470–4493.
[15] X. Gong, Y. Wang, T. Kuang, ZIF-8-based membranes for carbon dioxide capture and separation, ACS Sustain. Chem. Eng. 5 (2017) 11204–11214.
[16] Y.V. Kaneti, et al., Strategies for improving the functionality of zeolitic imidazolate frameworks: Tailoring nanoarchitectures for functional applications, Adv. Mater. 29 (2017) 1700213.
[17] K.S. Park, et al., Exceptional chemical and thermal stability of zeolitic imidazolate frameworks, Proc. Natl. Acad. Sci. 103 (2006) 10186–10191.
[18] R. Banerjee, et al., High-throughput synthesis of zeolitic imidazolate frameworks and application to CO_2 capture, Science. 319 (2008) 939–943.
[19] T. Li, Y. Pan, K.-V. Peinemann, Z. Lai, Carbon dioxide selective mixed matrix composite membrane containing ZIF-7 nano-fillers, J. Memb. Sci. 425–426 (2013) 235–242.
[20] L. Xiang, et al., Locking of phase transition in MOF ZIF-7: improved selectivity in mixed-matrix membranes for O_2/N_2 separation, Mater. Horizons. 7 (2020) 223–228.
[21] B. Seoane, J.M. Zamaro, C. Tellez, J. Coronas, Sonocrystallization of zeolitic imidazolate frameworks (ZIF-7, ZIF-8, ZIF-11 and ZIF-20), CrystEngComm 14 (2012) 3103–3107.
[22] M. García-Palacín, et al., Sized-controlled ZIF-8 nanoparticle synthesis from recycled mother liquors: Environmental impact assessment, ACS Sustain. Chem. Eng. 8 (2020) 2973–2980.
[23] Y. Pan, Y. Liu, G. Zeng, L. Zhao, Z. Lai, Rapid synthesis of zeolitic imidazolate framework-8 (ZIF-8) nanocrystals in an aqueous system, Chem. Commun. 47 (2011) 2071–2073.
[24] J. Qian, F. Sun, L. Qin, Hydrothermal synthesis of zeolitic imidazolate framework-67 (ZIF-67) nanocrystals, Mater. Lett. 82 (2012) 220–223.
[25] Y. Dai, J.R. Johnson, O. Karvan, D.S. Sholl, W.J. Koros, Ultem®/ZIF-8 mixed matrix hollow fiber membranes for CO_2/N_2 separations, J. Memb. Sci. 401–402 (2012) 76–82.
[26] M.R. Hasan, L. Paseta, M. Malankowska, C. Téllez, J. Coronas, Synthesis of ZIF-94 from recycled mother liquors: Study of the influence of its loading on post-combustion CO_2 capture with Pebax based mixed matrix membranes, Adv. Sustain. Syst. 6 (2022) 2100317.
[27] L. Xiang, L. Sheng, C. Wang, L. Zhang, Y. Pan, Y. Li, Amino-functionalized ZIF-7 nanocrystals: Improved intrinsic separation ability and interfacial compatibility in mixed-matrix membranes for CO_2/CH_4 separation, Adv. Mater. 29 (2017) 1606999.
[28] S. Japip, Y. Xiao, T.-S. Chung, Particle-size effects on gas transport properties of 6FDA-Durene/ZIF-71 mixed matrix membranes, Ind. Eng. Chem. Res. 55 (2016) 9507–9517.
[29] M. Safak Boroglu, A.B. Yumru, Gas separation performance of 6FDA-DAM-ZIF-11 mixed-matrix membranes for H_2/CH_4 and CO_2/CH_4 separation, Sep. Purif. Technol. 173 (2017) 269–279.
[30] Z. Wang, et al., ZIF-301 MOF/6FDA-DAM polyimide mixed-matrix membranes for CO_2/CH_4 separation, Sep. Purif. Technol. 264 (2021) 118431.
[31] J. Yuan, H. Zhu, J. Sun, Y. Mao, G. Liu, W. Jin, Novel ZIF-300 mixed-matrix membranes for efficient CO_2 capture, ACS Appl. Mater. Interfaces 9 (2017) 38575–38583.
[32] J. Guan, et al., Design and prediction of metal organic framework-based mixed matrix membranes for CO_2 capture via machine learning, Cell Reports Phys. Sci. 3 (2022).
[33] R. Thür, et al., Correlating MOF-808 parameters with mixed-matrix membrane (MMM) CO2 permeation for a more rational MMM development, J. Mater. Chem. A 9 (2021) 12782–12796.
[34] S. Meshkat, S. Kaliaguine, D. Rodrigue, Comparison between ZIF-67 and ZIF-8 in Pebax® MH-1657 mixed matrix membranes for CO_2 separation, Sep. Purif. Technol. 235 (2020) 116150.
[35] M. van Essen, et al., The influence of pore aperture, volume and functionality of isoreticular gmelinite zeolitic imidazolate frameworks on the mixed gas CO_2/N_2 and CO_2/CH_4 separation performance in mixed matrix membranes, Sep. Purif. Technol. 260 (2021) 118103.
[36] J. Sánchez-Laínez, et al., Influence of ZIF-8 particle size in the performance of polybenzimidazole mixed matrix membranes for pre-combustion CO_2 capture and its validation through interlaboratory test, J. Memb. Sci. 515 (2016) 45–53.
[37] R.J. Verploegh, A. Kulkarni, S.E. Boulfelfel, J.C. Haydak, D. Tang, D.S. Sholl, Screening diffusion of small molecules in flexible zeolitic imidazolate frameworks using a DFT-parameterized force sield, J. Phys. Chem. c. 123 (2019) 9153–9167.
[38] Q. Jia, E. Lasseuguette, M.M. Lozinska, M.-C. Ferrari, P.A. Wright, Hybrid Benzimidazole-dichloroimidazole zeolitic imidazolate frameworks based on ZIF-7 and their application in mixed matrix membranes for CO_2/N_2 separation, ACS Appl. Mater. Interfaces 14 (2022) 46615–46626.
[39] L.H. Wee, et al., Chlorination of a zeolitic-imidazolate framework tunes packing and van der Waals interaction of carbon dioxide for optimized adsorptive separation, J. Am. Chem. Soc. 143 (2021) 4962–4968.
[40] Q. Hou, Y. Wu, S. Zhou, Y. Wei, J. Caro, H. Wang, Ultra-tuning of the aperture size in stiffened ZIF-8_Cm frameworks with mixed-linker strategy for enhanced CO_2/CH_4 separation, Angew. Chemie Int. Ed. 58 (2019) 327–331.
[41] W. Morris, et al., A combined experimental-computational study on the effect of topology on carbon dioxide ddsorption in zeolitic imidazolate frameworks, J. Phys. Chem. C 116 (2012) 24084–24090.
[42] A.M. Marti, S.R. Venna, E.A. Roth, J.T. Culp, D.P. Hopkinson, Simple fabrication method for mixed matrix membranes with in situ MOF growth for gas separation, ACS Appl. Mater. Interfaces 10 (2018) 24784–24790.
[43] X. Ma, X. Wu, J. Caro, A. Huang, Polymer composite membrane with penetrating ZIF-7 sheets displays high hydrogen permselectivity, Angew. Chemie Int. Ed. 58 (2019) 16156–16160.
[44] R. Castro-Muñoz, V. Martin-Gil, M.Z. Ahmad, V. Fíla, Matrimid® 5218 in preparation of membranes for gas separation: Current state-of-the-art, Chem. Eng. Commun. 205 (2018) 161–196.
[45] A.S. Embaye, L. Martínez-Izquierdo, M. Malankowska, C. Téllez, J. Coronas, Poly (ether-block-amide) copolymer membranes in CO_2 separation applications, Energy & Fuels 35 (2021) 17085–17102.
[46] Q. Song, et al., Zeolitic imidazolate framework (ZIF-8) based polymer nanocomposite membranes for gas separation, Energy Environ. Sci. 5 (2012) 8359–8369.
[47] N.L. Torad, et al., Facile synthesis of nanoporous carbons with controlled particle sizes by direct carbonization of monodispersed ZIF-8 crystals, Chem. Commun. 49 (2013) 2521–2523.
[48] M. Etxeberria-Benavides, et al., High performance mixed matrix membranes (MMMs) composed of ZIF-94 filler and 6FDA-DAM polymer, J. Memb. Sci. 550 (2018) 198–207.
[49] A. Khoshkharam, N. Azizi, R.M. Behbahani, M.A. Ghayyem, Separation of CO_2 from CH_4 using a synthesized Pebax-1657/ZIF-7 mixed matrix membrane, Pet. Sci. Technol. 35 (2017) 667–673.
[50] W. Zheng, R. Ding, K. Yang, Y. Dai, X. Yan, G. He, ZIF-8 nanoparticles with tunable size for enhanced CO_2 capture of Pebax based MMMs, Sep. Purif. Technol. 214 (2019) 111–119.
[51] R. Lin, B. Villacorta Hernandez, L. Ge, Z. Zhu, Metal organic framework based mixed matrix membranes: an overview on filler/polymer interfaces, J. Mater. Chem. A 6 (2018) 293–312.
[52] E. Lasseuguette, L. Fielder-Dunton, Q. Jia, M.-C. Ferrari, The effect of solution casting temperature and ultrasound treatment on PEBAX MH-1657/ZIF-8 mixed matrix membranes morphology and performance, Membranes. 12 (2022) 6.
[53] A. Nuhnen, C. Janiak, A practical guide to calculate the isosteric heat/enthalpy of adsorption via adsorption isotherms in metal–organic frameworks, MOFs, Dalt. Trans. 49 (2020) 10295–10307.
[54] C. Han, Y. Yang, D.S. Sholl, Quantitatively predicting impact of structural flexibility on molecular diffusion in small pore metal-organic frameworks—A molecular dynamics study of hypothetical ZIF-8 polymorphs, J. Phys. Chem. C 124 (2020) 20203–20212.
[55] Y. Yang, D.S. Sholl, A systematic examination of the impacts of MOF flexibility on intracrystalline molecular diffusivities, J. Mater. Chem. A 10 (2022) 4242–4253.
[56] Q. Shi, et al., Effective CH_4 enrichment from N_2 by SIM-1 via a strong adsorption potential SOD cage, Sep. Purif. Technol. 230 (2020) 115850.
[57] G. Chaplais, et al., Impacts of the imidazolate linker substitution (CH_3, Cl, or Br) on the structural and adsorptive properties of ZIF-8, J. Phys. Chem. C 122 (2018) 26945–26955.
[58] R. Chandra, M. Nath, Facile synthesis of metal-organic framework (ZIF-11) and Ag NPs encapsulated-ZIF-11 composite as an effective heterogeneous catalyst for photodegradation of Methylene Blue, Appl. Organomet. Chem. 34 (2020) 5951.
[59] D. Fairen-Jimenez, S.A. Moggach, M.T. Wharmby, P.A. Wright, S. Parsons, T. Düren, Opening the gate: Framework flexibility in ZIF-8 explored by experiments and simulations, J. Am. Chem. Soc. 133 (2011) 8900–8902.
[60] T. Chokbunpiam, S. Fritzsche, C. Chmelik, J. Caro, W. Janke, S. Hannongbua, Gate opening effect for carbon dioxide in ZIF-8 by molecular dynamics – Confirmed, but at high CO_2 pressure, Chem. Phys. Lett. 648 (2016) 178–181.
[61] W. Morris, et al., A combined experimental−computational investigation of carbon dioxide capture in a series of isoreticular zeolitic imidazolate frameworks, J. Am. Chem. Soc. 132 (2010) 11006–11008.
[62] J.-R. Li, R.J. Kuppler, H.-C. Zhou, Selective gas adsorption and separation in metal–organic frameworks, Chem. Soc. Rev. 38 (2009) 1477–1504.
[63] J. Liu, et al., Superhydrophobic zeolitic imidazolate framework with suitable SOD cage for effective CH_4/N_2 adsorptive separation in humid environments, AIChE J. 68 (2022) 17589.
[64] G. Yue, H. Wu, J. Yue, M. Li, C. Zeng, W. Liang, Adsorption measurement and dual-site Langmuir model II: Modelling and prediction of carbon dioxide storage in coal seam, Energy Explor. Exploit. 37 (2019) 1268–1285.

[65] S. Gadipelli, W. Travis, W. Zhou, Z. Guo, A thermally derived and optimized structure from ZIF-8 with giant enhancement in CO_2 uptake, Energy Environ. Sci. 7 (2014) 2232–2238.
[66] P. Pandey, R.S. Chauhan, Membranes for gas separation, Prog. Polym. Sci. 26 (2001) 853–893.
[67] Q. Zhao, S. Lian, R. Li, Y. Yang, G. Zang, C. Song, Fabricating leaf-like hierarchical ZIF-67 as intra-mixed matrix membrane microarchitecture for efficient intensification of CO_2 separation, Sep. Purif. Technol. 305 (2023) 122460.
[68] Y. Cheng, et al., Mixed matrix membranes containing MOF@COF hybrid fillers for efficient CO_2/CH_4 separation, J. Memb. Sci. 573 (2019) 97–106.
[69] Q. Jia, E. Lasseuguette, M.-C. Ferrari, P.A. Wright, 2024, Comparison of the effect of topology type and linker composition of zeolitic imidazolate framework fillers on the performance of mixed matrix membranes in CO_2/N_2 separation. Dataset. University of St Andrews Research Portal. https://doi.org/10.17630/15eb2536-4610-4943-8edd-28361816f0c8.